

## **2.1 Materials**

## **2.2 Membrane Synthesis**

## **2.3 Membrane Characterization**

### **2.3.1 Gas Permeability Set- Up**

### **2.3.2 Diffusion Coefficients and Solubility Coefficients**

### **2.3.3 Porosity Analysis**

### **2.3.4 Differential Scanning Calorimetry (DSC)**

### **2.3.5 Thermalgravimetric Analyzer (TGA)**

### **2.3.6 Fourier Transform Infrared (FT-IR) Spectroscopy**

### **2.3.7 Mechanical Properties**

### **2.3.8 X-ray Diffraction**

### **2.3.9 Field Emission Scanning Electron Microscopy (FE-SEM) Analysis**

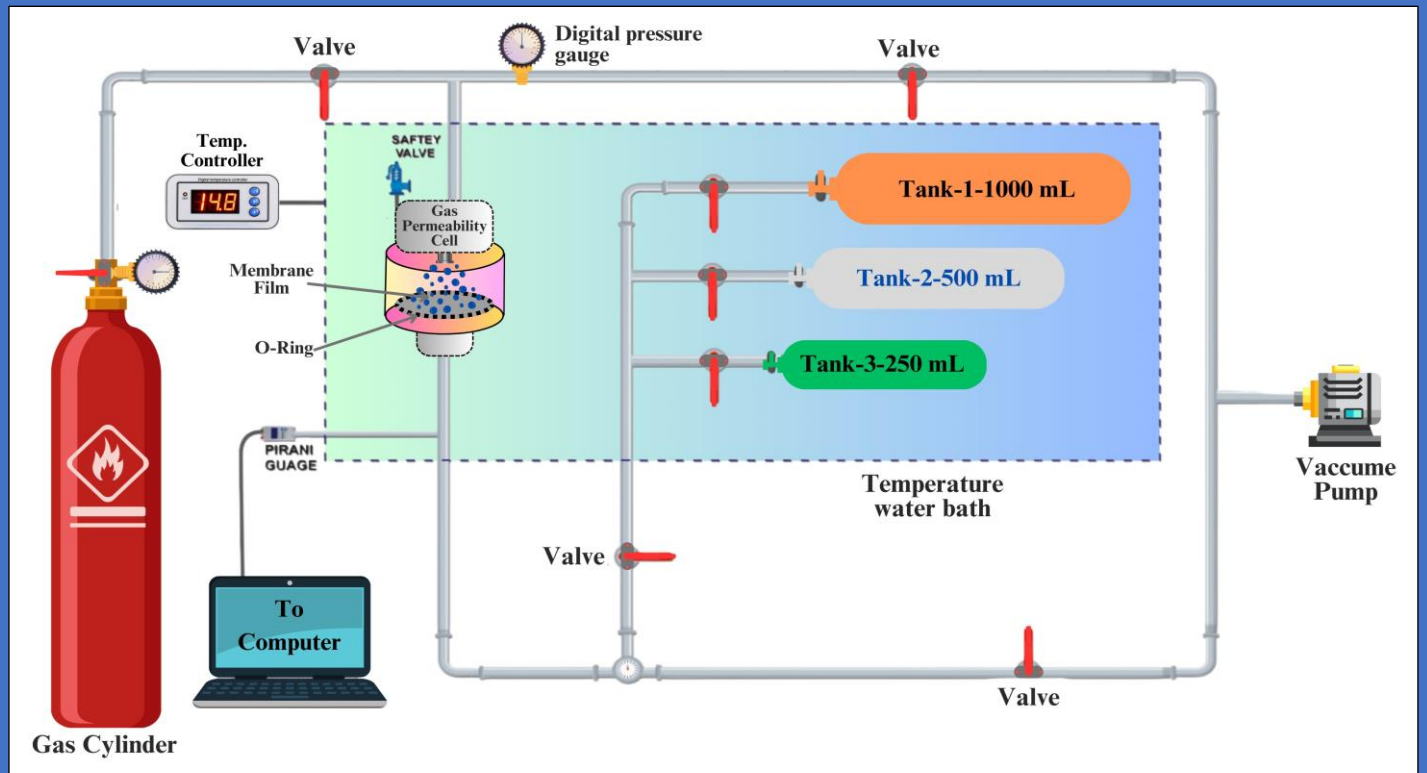
### **2.3.10 UV-Visible Spectroscopy**

### **2.3.11 Contact Angle Analysis**

## **References**

# Chapter - 2

## *Experimental*



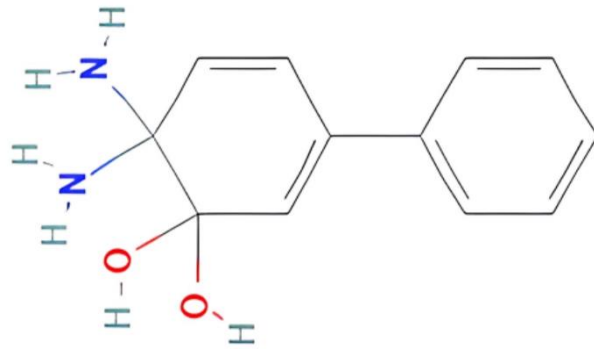
The present chapter 2 describes the material used for research work and methodologies of membrane synthesis and their characterization techniques. The experimental involves membrane synthesis process, gas permeation test and other standard characterization techniques. The information regarding to the analytic instruments and their sources are explained in this chapter. The synthesis of membrane materials is explained by variety of modifications such as blend polymer membranes, nanofiller dispersed composite and blend composite membranes. Gas transport through of membrane materials is described by using single gas permeation test under fixed test conditions. In this chapter, we discussed different characterization methods.

### 2.1 Materials

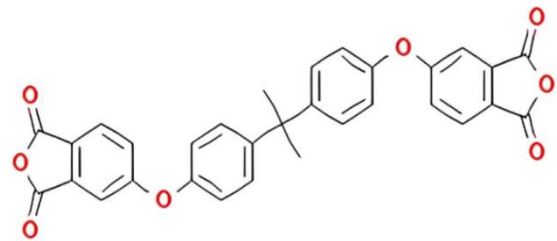
*Polymer used in present thesis:* Aromatic diamine, 3,30 -dihydroxy-4,40 -diamino-biphenyl (HAB), and dianhydride, 2,20-bis-(3,4-dicarboxyphenyl) hexafluoropropylene dianhydride (6FDA), was purchased from Chriskev Company (USA). Fluoro polymer Industries Pvt. Ltd., Vadodara, provided Polymethyl Methacrylate (PMMA) and Polystyrene (PS). Polyethylene terephthalate (PET) and Polyethylene glycol (PEG) provided by Parshwa Polymer Industries, Mumbai, India. Polydimethylsiloxane (PDMS) was purchased from Sigma-Aldrich.

*The solvents:* N-methyl-2-pyrrolidone (NMP) was dissolvable through vacuum refining with calcium hydride, dimethylacetamide (DMAc), Acetone, Toluene and Tetrahydrofuran (THF), Chloroform ( $\text{CHCl}_3$ ), was purchased from Durga Scientific Private Limited, Vadodara, Gujarat, India.

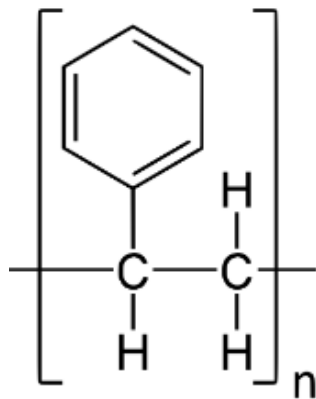
*The nanofillers:* Graphene Oxide nanofillers (GO, Purity > 99%, 30-40 nm in diameter, 20-25  $\mu\text{m}$  in length), Titanium dioxide ( $\text{TiO}_2$ , purity > 99%, 10-15 nm, nm in diameter, 5-10  $\mu\text{m}$  in length), Carbon Nanotubes (CNT, purity > 95% 10-20 nm in diameter, 5-15  $\mu\text{m}$  in length) were purchased from Platonic Nanotechnology Lab, Jharkhand, India. Silica nanoparticles (stock number 4860MR) were supplied by Nanostructure and Amorphous Materials, Inc, Houston, USA.



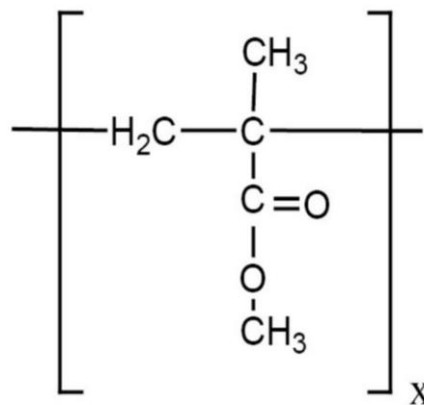
3,3'-dihydroxy-4,4'-diamino-biphenyl (HAB)



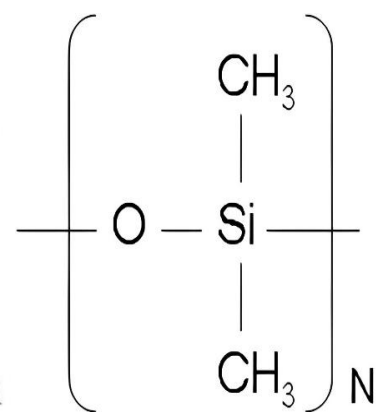
Hexafluoropropylene dianhydride (6FDA)



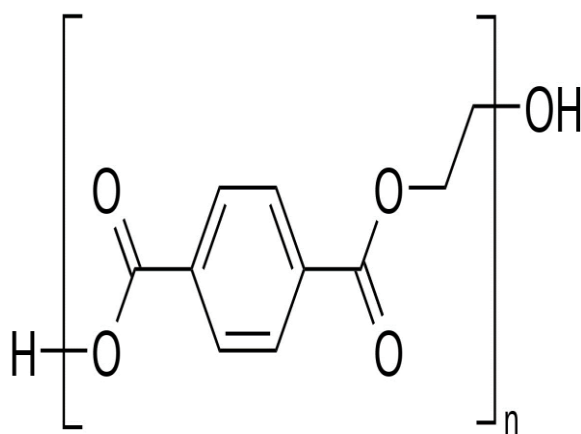
Polystyrene (PS)



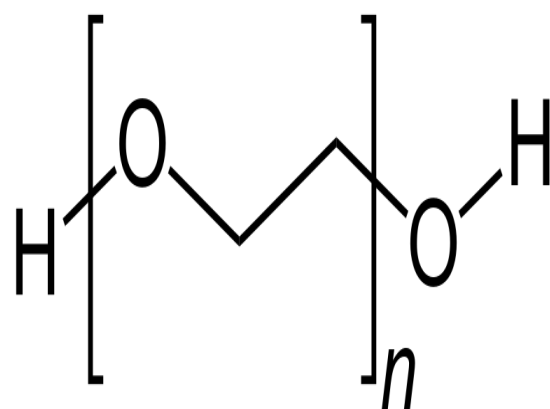
Polymethyl Methacrylate (PMMA)



Polydimethylsiloxane (PDMS)



Polyethylene terephthalate (PET)



Polyethylene glycol (PEG)

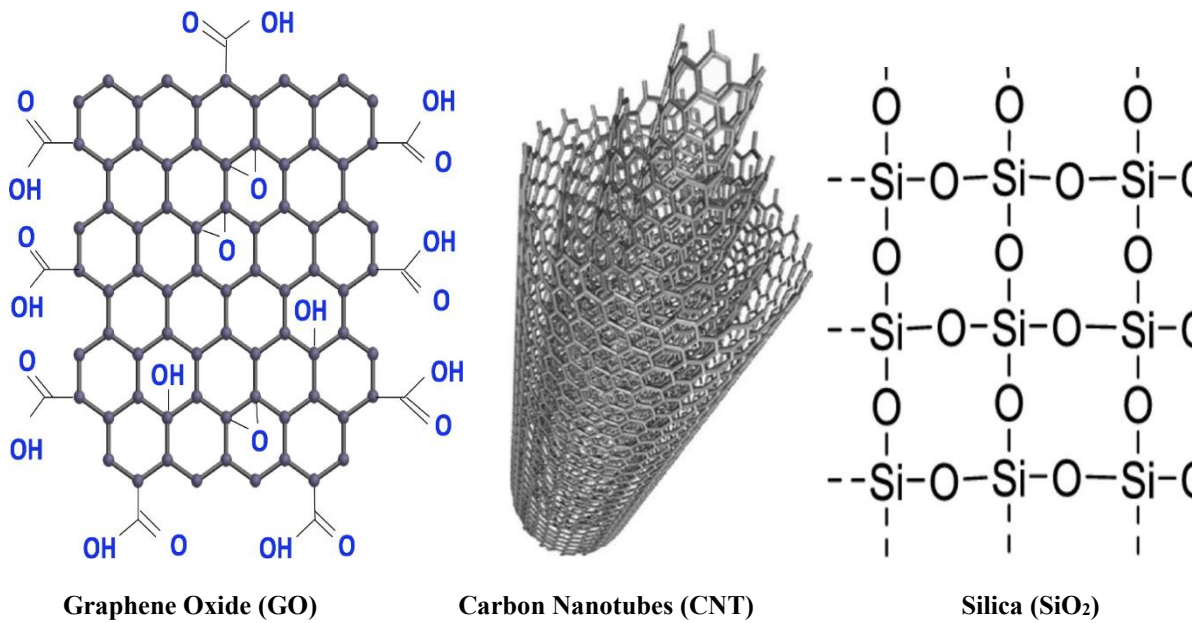


Figure 2.1: Chemical structures of the Polymer and Nanofillers

## 2.2 Membrane Synthesis

Variety of the membrane were prepared using solution casting method. It involves the preparation of a solution of a polymer in a suitable solvent, followed by casting or spreading this solution onto a substrate to form a membrane. The solvent is then allowing to evaporate, leaving behind the solid polymer membranes [1].

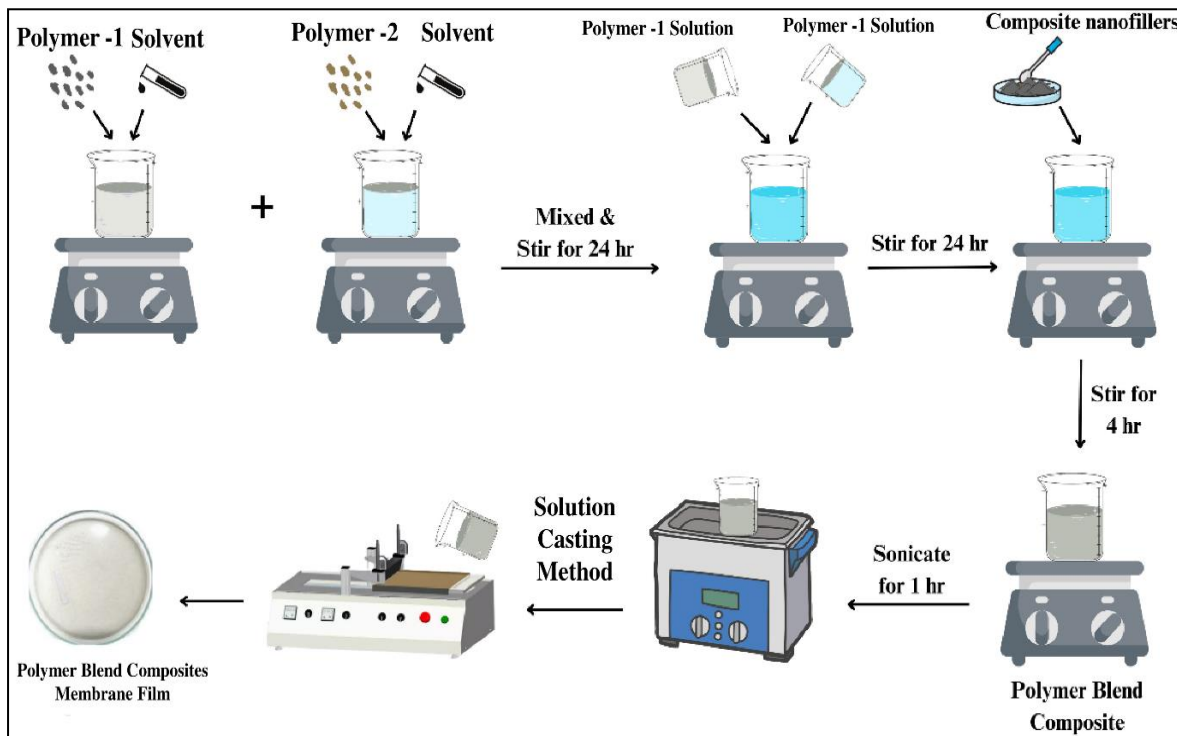


Figure 2.2: Preparation of membrane with different nanofillers using the solution casting method

As shown in Figure 2.2 the Polymer 1 and Polymer 2 both the polymers are dissolved in a suitable solution of in this process. The different nanoparticles were dispersed in the same solution, whereas the polymer matrix phase was readily dissolvable. The blend of polymeric membranes with nanofillers was prepared by the solution casting method. A magnetic stirrer was used to mix these polymers for their blend and composite blend with nanofillers [2]. The common solvent used for synthesizing these pure, blended, and blended composite membrane membranes. To get a homogenous solution, the solution of Polymer 1 and Polymer 2 and blend composite with nanofillers was individually stirred for 3 hr in a solvent, and then went the mixture of these blend composite was sonicated for 1 hr by using prob-sonicator to protect agglomeration and then entire solution was again stirred for 24 hr at ambient temperature. On a flat bottomed glass, the mixture was transferred, and the solvent was allowed to evaporate overnight. The permeability of these membranes was tested the next day after they were peeled-off from the petri dish has to measure the thickness of casted membrane. A thickness gauge with a least count of 0.001 mm. Approximate thickness between 65  $\mu\text{m}$  to 70  $\mu\text{m}$  were used for characterization [3]. A schematic procedure of the solution casting technique for the synthesizing of homogeneous polymer blend composites membranes is shown in Figure 2.2.

## **2.3 Membrane Characterization**

### **2.3.1 Gas Permeability Set- Up**

In order to measure the permeability of  $\text{H}_2$ ,  $\text{CO}_2$ ,  $\text{O}_2$ ,  $\text{N}_2$ , and Ar, is measured through a constant pressure/variable volume system. Transport properties of a membranes is important tool to investigate the membrane behaviour. Qualitative and quantitative has permeability studies are performed. This system was used from the downstream side of the gas permeability cell and the output of the gas was measured as a function of volume change with time. The schematic diagram of set-up shown in Figure 2.4 and Figure 2.5 [4]. To calculate the amount of gas being carried at a given rate, a pressure transducer was used. A gas permeation cell made of stainless steel and a mercury flowmeter has been set up in our lab.

The output obtained by the constant pressure/variable volume system was recorded as function of change of volume with respect to time from downstream side of the gas permeability cell. Gas permeability cell is key part for this developed system made of two cylinders of stainless steel 316 material as shown in the Figure 2.3. Towards the feed side, a pressure gauge was attached providing maximum pressure up to 150 psi and  $V_1$  represents the inlet valve to feed the gas inside the cell. Valve  $V_2$  was used for purging gas or the air impurities

from the inert volume of the cell [5]. The cell has been developed with taper threading to connect the valves, pressure gauge and outlet nozzle. Especially for the gas testing applications, taper threading at joining parts gives better clearance to prevent gas leakage from the system. Membrane was placed inside the lower cylinder with porous support. Two distinct diameter O-rings were placed inside the lower cylinder concentrically to conform accurate test measurement providing necessary seal. Larger O-ring was used to seal the cell, creating leak free seal at the connecting edges of both the cylinders. In order to prevent feed gas escaping directly from feed side in to downstream phase, smaller one was used to create seal on the surface of test membrane. The function of O-ring at the connecting edges is to create seal between gas flux from upstream and downstream side. The central O-ring is of same diameter of central outlet to prevent gas flow from the membrane edge. Silicone grease was used to apply on the surface of O-rings to ensure adhesion against higher pressure. Both the cylinders of gas permeability cell were sealed with six fully threaded hex screws [6].

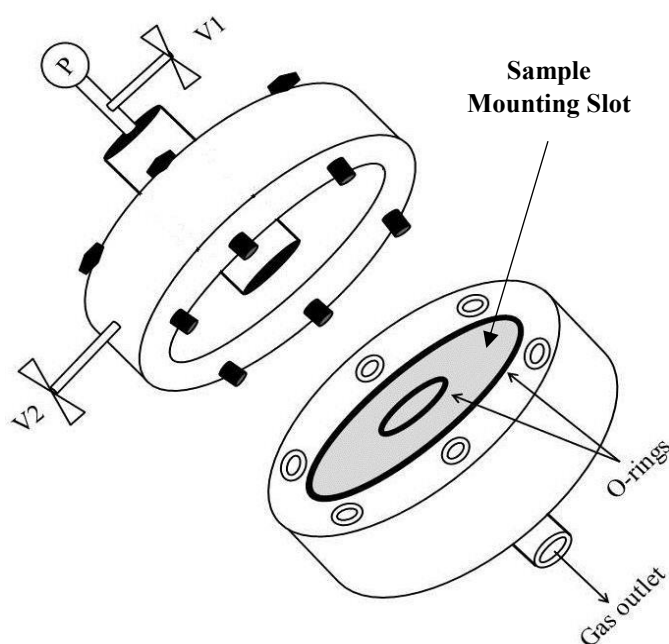


**Figure 2.3:** Schematic diagram of gas permeability cell

Constant pressure/variable volume method works well with membrane to obtain permeability. Gas flux that has penetrated the downstream volume of the gas permeability cell is connected to the mercury flowmeter depends on the membrane material used for the analysis [7]. The rate of gas volume penetration through membrane is calculated from a plot of mercury slug height against time using the slope  $dh/dt$  multiplied by the capillary area 'a', that provide the amount of gas passes.

Single gas permeability is calculated using the following equation (2.1),

$$P = \frac{l}{P_1 - P_2} \cdot \frac{P_{atm}}{ART} \cdot a \cdot \frac{dh}{dt} \quad (2.1)$$

The rate of gas flow across the membrane is measured by  $(P_1 - P_2)$ ,  $(P_1 - P_2)$  is the pressure where difference between the upstream and downstream sides of the membrane, and  $l$  the thickness of the membrane in centimeters (cm).  $A$  is the membrane's cross sectional area in  $\text{cm}^2$ ,  $P_{atm}$  is atmospheric pressure ( $1 \text{ atm} = 76 \text{ Hg.cm}$ ). The temperature  $T$  is measured in  $^\circ\text{C}$ ,  $R$  is the universal gas constant and the gas permeability of this system was measured in Barrer. Glassy polymers were used for the study of polymer materials conducting the test, a small amount of leakage cannot be minimized [8].

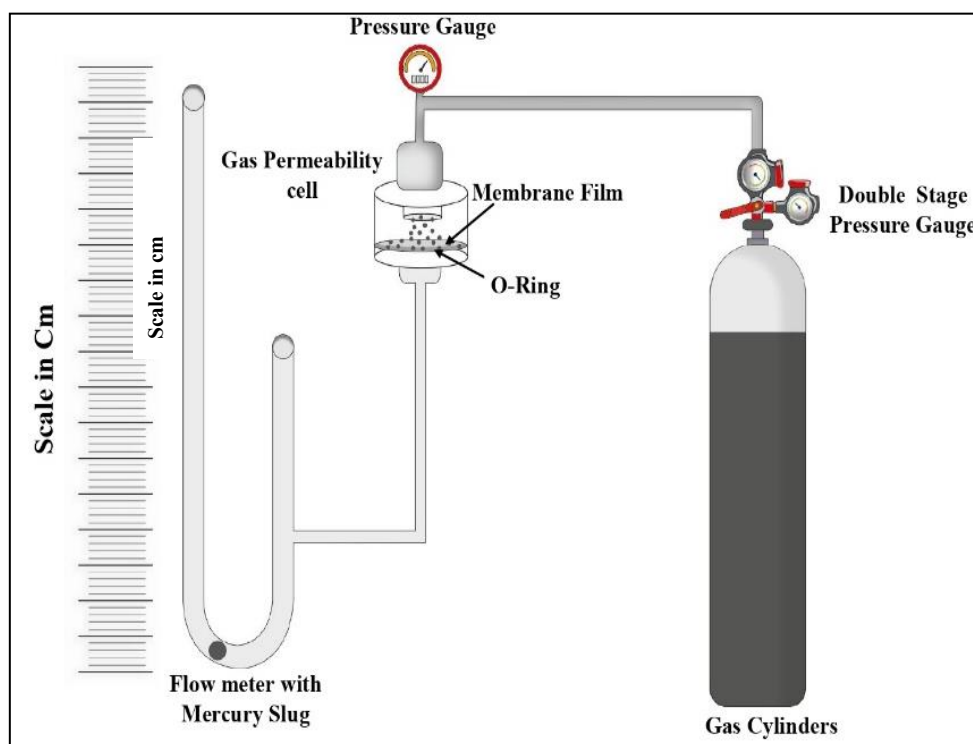
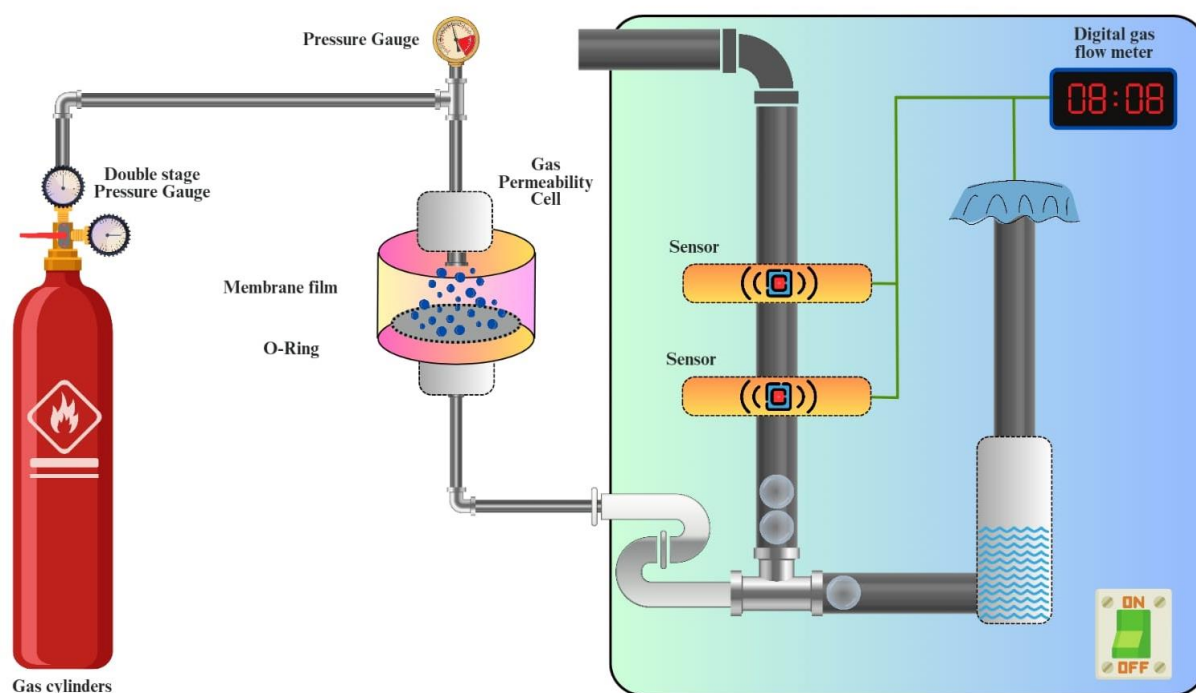


Figure 2.4: Schematic diagram of constant pressure/variable volume system

An experiment was performed using flat non porous rubber sheet, this rubber sheet placed at membrane cell at 30 psi upstream pressure for 48 hr with air acting as the penetrant to check for system leakage. No pressure change occurred, and the height of the mercury slug remained constant for two days. It indicates that rubber sheet does not penetrate the molecules of the air in less than 48 hr [9]. Now by using aluminium foil, samples were that provide the appropriate exposed size. Membrane was mounted between aluminium foil and placed in a membrane cell. As shown in the Figure 2.4 the feed gas supplied by gas cylinder enters through the valve connected between the cylinder and feed side of the gas permeability cell. Before

beginning the measurements, upstream and the downstream sides were purged with the feed gas twice to remove any impurities and to achieve better transport rate of the applied gas. The target gas was supplied at constant pressure towards upstream face of the membrane and steady-state gas flux was measured from the downstream side of the membrane in the mercury flowmeter. The rate of change of the gas molecules transported through the membrane and record the movement of the mercury slug inside the capillary of the flowmeter which was attached with the height scale. Initially, mercury slug was set at particular height at the upper side of the curved portion of the flowmeter using a bubbler through the opening valve. The system was degassed twice using the feed gas before starting the experiment for accurate measurements. The gas molecules permeated through the membrane towards downstream side flows within the mercury flowmeter. As the gas expanded in to the flowmeter capillary containing mercury slug, displaced upward as the permeated gas pushed it. Its movement offers direct measurement of gas flux permeating through the membrane.



**Figure 2.5:** Schematic of bubble flow meter-based system with constant pressure/variable volume

A bubble flow meter has been used in the constant pressure/variable volume system to measure the rate of flow of gas molecules, which is shown in Figure 2.5. The feed gas supplied by the gas cylinder is allowed to flow via the valve that joins it to the feed side of the gas permeability cell. Now that the target gas has been injected at 30 psi constant pressure towards the membrane's upstream face.

The bubble flow meter has been used to measure the steady state gas flux from the downstream side of the membrane. The bubble flow meter would display the rate of volume change over time for each distinct bubble on the screen if we could only reach one bubble at the top of the capillary tube, permitting us to monitor only one bubble [10].

The gas molecules move through the membrane of the bubble flow meter to the downstream side flows. The experiment has been performed several times to get an accurate measurement. The following equation (2.2) has been used to determine the permeability of the system in a steady state:

$$P = \frac{l}{P_1 - P_2} \times \frac{P_{atm}}{ART} \times \frac{dv}{dt} \quad (2.2)$$

The pressure difference across the membrane's upstream and downstream sides is ( $P_2 - P_1$ ),  $P_1$  is sufficiently small compared to  $P_2$ , therefore, we can only consider  $P_2$  in the calculation. Where  $dv/dt$  is the rate of change in gas flow that penetrates the membrane,  $A$  is the membrane's cross sectional area in  $\text{cm}^2$ ,  $P_{atm}$  is atmospheric pressure ( $1 \text{ atm} = 76 \text{ Hg.cm}$ ), and  $l$  is the membrane's thickness in  $\text{cm}$ . The temperature  $T$  is measured in  $^\circ\text{C}$ , whereas the universal gas constant  $R$  is expressed in  $\text{cmHg.cm}^3/(\text{STP}) \text{ cm}^3 \text{ K}$ . This system determined the unit Barrer for gas permeability measurement.

### 2.3.2 Diffusion Coefficients and Solubility Coefficients

By measuring a penetrant's diffusivity, one may determine how quickly it diffuses into a membrane matrix. Small gas molecules diffuse into the polymeric medium and functionalize the polymer [11]. Diffusivity indicates the transport rate of penetrant within membrane matrix. Diffusion coefficient is influenced by various factors such as: (a) Physical state and molecular size of penetrant, (b) Penetrant compatibility with polymer matrix, (c) Membrane morphology and (d) Interfacial energy of membrane structure [12]. Diffusion through polymer membrane depends on the polymer free volume and its segmental mobility. The shape of diffusive gas molecule should not be ignored while discussing about diffusion coefficient as the spherical gas molecule diffuses faster compared to linear, elongated and flattened molecule. For gas molecules having weak interactions with polymer composition, diffusion coefficient is independent of gas concentration. The diffusion of gas molecules in the glassy polymer membrane follows Fick's law of diffusion.

According to this law gas flux passing through the membrane is directly proportional to concentration gradient:

$$J = -D \frac{dc}{dx} \quad (2.3)$$

In equation (2.3),  $dc/dx$  is the concentration gradient. The determination of diffusion coefficient can be performed by time lag interpretation. As the fed gas has applied at constant operating pressure to the membrane inside closed volume system, the gas permeates due to concentration gradient.

The initial transient regime is considered as time lag denoted by  $\theta$ , the relation between time lag and diffusion coefficient is given in below equation (2.4):

$$D = \frac{l^2}{6\theta} \quad (2.4)$$

Where,  $l$  is the membrane thickness and unit of diffusion coefficient is  $\text{cm}^2/\text{s}$ .

It is defined as the amount of gas molecules sorbed by the membrane. It is also called sorption coefficient, which is thermodynamic parameter. As it is related to specific interactions between penetrant and polymer, it is influenced by gas condensability, free volume distribution and distribution of electron density in the polymer matrix. Solubility increases as the interaction between a gas and polymer functional group becomes stronger. e.g.  $\text{CO}_2$  being polar molecule, is much soluble in polymers having polar functional groups. Solubility coefficient can be determined by the permeability-diffusivity relation as per given in equation (2.5):

$$S = \frac{P}{D} \quad (2.5)$$

The unit of solubility is  $\text{cm}^3$  (STP)/ $\text{cm}^3 \cdot \text{cmHg}$ .

### 2.3.3 Porosity Analysis

The porosity of the membrane was assessed using the dry-wet weight method. 3 cm by 3 cm membrane samples was cut out and immersed in water for a night. The weight was measured while soaking on an analytical balance with accuracy. The membrane was removed and the water on its surface was gently cleaned off with filter paper after being soaked in distilled water for 24 hr at room temperature. The membrane samples were then allowed to dry at room temperature for a whole night before being measured the following morning to determine their dry weight. All weights were regularly recorded on an analytical balance, and

a digital thickness meter with accuracy of  $\pm 1 \mu\text{m}$  was used to measure the sample thickness twice on each side [12]. Using the information and the subsequent equations (2.6), the porosity was then calculated as follow:

$$\alpha = \frac{W_{\text{wet}} - W_{\text{dry}}}{a \cdot t \cdot \rho} \quad (2.6)$$

Where  $\alpha$  = membrane porosity (%), weights are expressed as  $W_{\text{wet}}$  (g) for the wet membrane and  $W_{\text{dry}}$  (g) for the dry membrane,  $a$  = membranes effective surface area ( $\text{cm}^2$ ),  $t$  = membrane's thickness ( $\mu\text{m}$ ), and  $\rho$  = water density ( $\text{g}/\text{cm}^3$ ).

The determination of porosity by the dry-wet weight technique is a method used to calculate the porosity of a material, especially in the context of porous media like soils or films. The porosity of a material represents the void spaces or openings within it and is expressed as a percentage.

### 2.3.4 Differential Scanning Calorimetry (DSC)

The schematic diagram of differential scanning calorimetry is shown in the Figure 2.6. The reference and the sample holder are placed inside the heat sink which is surrounded by heater. Any temperature difference in the reference and sample can be obtained by the heat flux recording. DSC measures the temperature and heat flow associated with the transitions in the material as a function of time and temperature. These measurements provide information about the physical and chemical changes which involve endothermic or exothermic reaction occur during the analysis [13]. It analyses the endothermic (heat flows into sample) and exothermic (heat flows out of the sample) transitions within the sample as a function of temperature. From DSC measurement, glass transition temperature ( $T_g$ ) of the membrane or other amorphous sample can be determined, which reveals the polymer intrinsic properties. A polymer can be classified as a glassy or rubbery based on their  $T_g$  values. The shift in the  $T_g$  values offers the information about the change in thermal characteristics of the sample. When the rubbery polymer material is placed at above temperature beyond its  $T_g$  value it becomes flexible and at lower temperature it becomes hard and brittle.

The measured melting temperature ( $T_m$ ) values explain the polymer crystalline and amorphous nature based on their polymer chain conformations and free volume. The instrument contains two pan which uses for sample and other one for the reference. Both pan have heaters with sensors which indicates the temperature values at higher to lower temperature

analysis. The heat flow can be measured as exothermic or endothermic with respect to temperature. The heat flow versus temperature plot yield the information of physical properties of the sample (Figure 2.6). The thermal analysis and glass transition temperature of pure and blends polymers were obtained using a DSC-25 (TA Instruments) USA, in our department, which shows in Figure 2.6 (b).

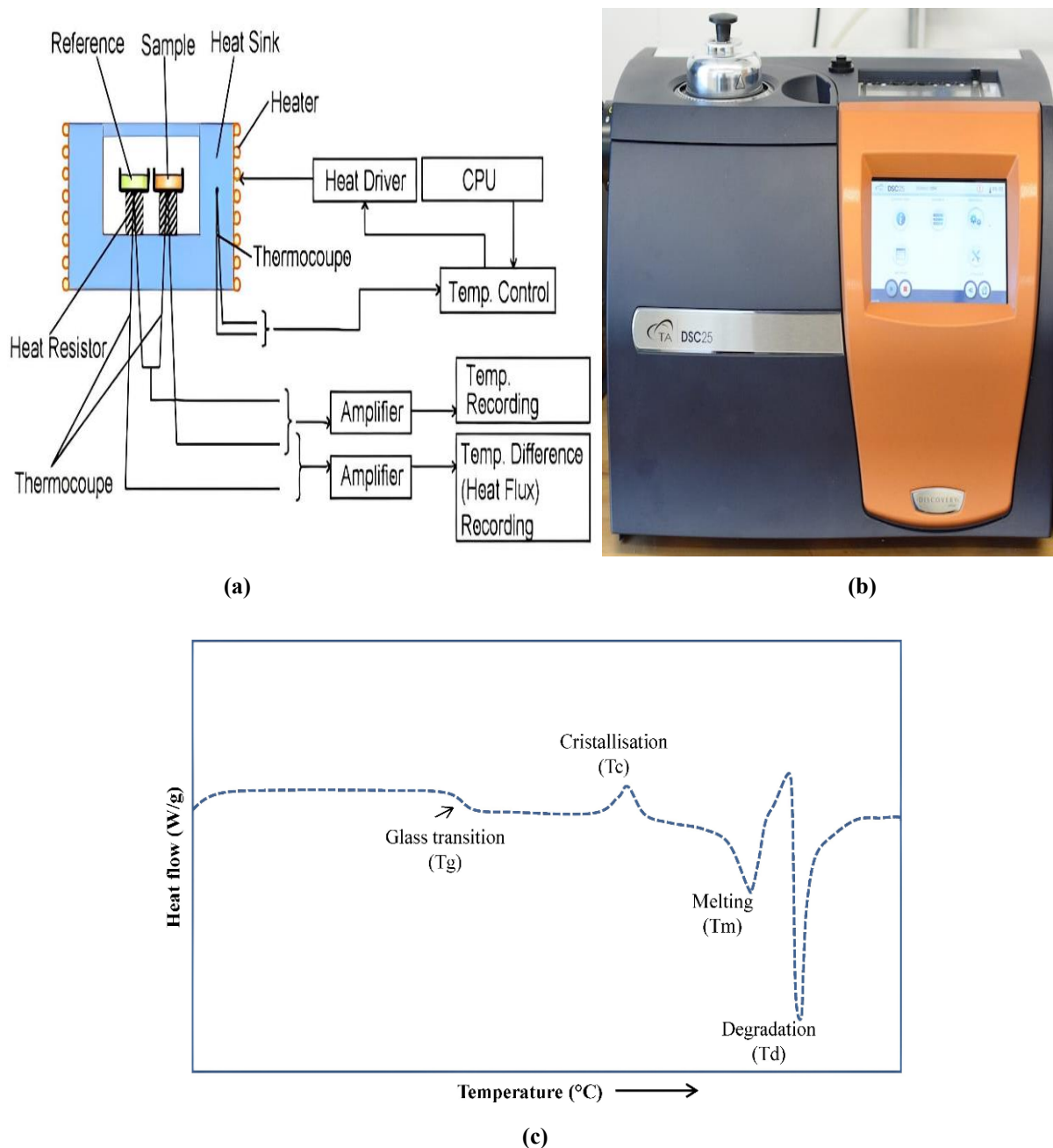


**Figure 2.6:** (a) Schematic diagram of DSC (b) DSC instrument (c) DSC spectrum

Scanning of membrane material with different heating rates like 5 °C/min, 10 °C/min and 20 °C/min. The TRIOS software was used to find glass transition temperatures and heat capacity of the membrane material. Small bits of thin polymer membrane were cut and placed

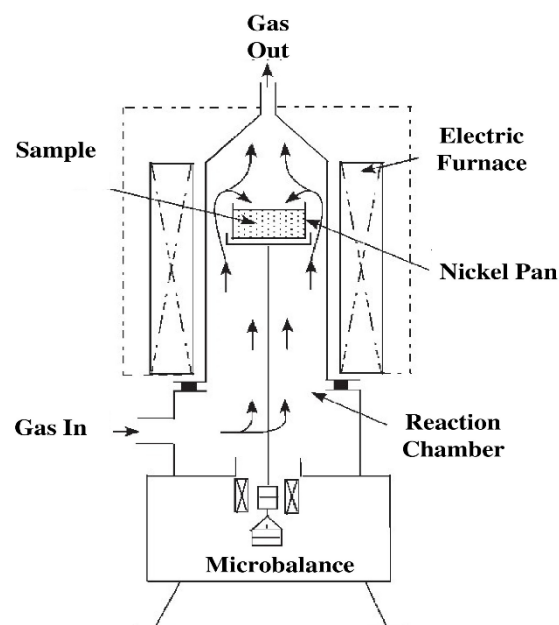
in aluminum pans. A micro weight balance was used to weight the samples [14]. The exact process of the sample was tested four or three times, each time with a different heating rate and sample from the batch. The detailed analysis about glass transition temperature ( $T_g$ ) determined by the presented instrument will be discussed in susceptible chapters.

### 2.3.5 Thermalgravimetric Analyzer (TGA)

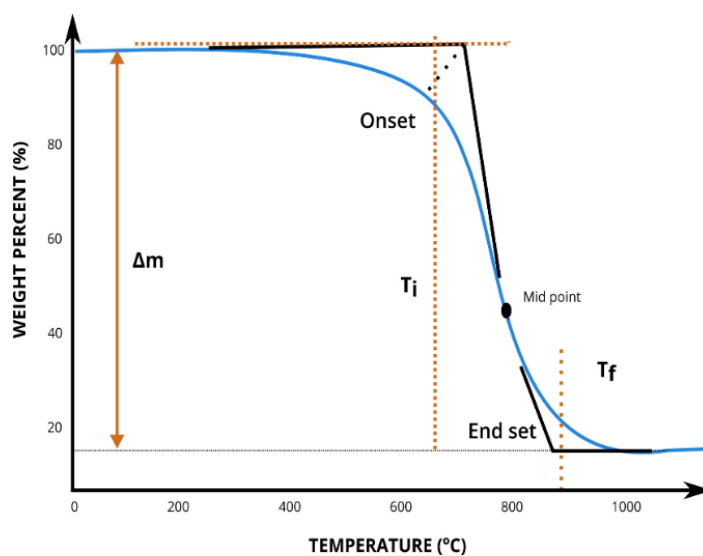
Thermalgravimetric analyzer (TGA) analysis is a prominent analytical tool to study the physical and chemical changes in the substance with respect to mass versus temperature.



(a)



(b)



(c)

Figure 2.7: (a) TGA instrument and (b) Schematic diagram of TGA instrument (c) TGA spectrum

The change in the weight of the substance as a function of temperature can be studied to evaluate the thermal stability, rate of reaction, reaction processes and specimen composition. The thermal stability of polymeric membranes prepared by different compositions and polymer materials can be analysed and used for the various applications on the basis of their thermal stability. Thermalgravimetric analyzer (TGA) thermal analysis modules. The weight loss mechanism involves the decomposition of the substance by breaking of chemical bonds followed by evaporation of volatile at higher temperature and reduction i.e. interaction of the sample to a reducing atmosphere [15]. The mass loss analysis of membranes were obtained using a TGA-550 (TA Instruments) USA, in our faculty, as shown in Figure 2.7 (b). Instrumentation and method of analysis are almost the same but the TGA only measures the weight changes upon heating at a constant rate. The working principle of TGA is that the mass of a substance is directly related to its chemical composition and physical structure. By heating the substance and measuring the changes in its mass over time, it is possible to determine the physical and chemical nature of the substance. In TGA, the weight of the sample changes at an increasing temperature at a constant rate with the atmospheric conditions and pressure remain constant.

Thermal decomposition (Td), refers to a chemical process where substances break down under elevated temperatures. The temperature at which this breakdown occurs is termed the decomposition temperature of the substance. Energy, typically in the form of heat, is necessary to disrupt the chemical bonds within the substance undergoing decomposition, resulting in a reaction that often requires input of heat, making it endothermic. Thermal decomposition reactions occur at high temperatures, during which the reactants absorb significant amounts of energy as they break down into simpler components. The reactant, which is the initial chemical entity, undergoes decomposition to yield simpler products.

Thermal stability that is the fingerprint thermograms and trends of thermal decomposition explain the thermal stability of the compounds and activation energy it give the information about the given sample by values at which the mass changes [16]. This technique analyses changes in a specimen's weight as its temperature increases. As a sample specimen has put through a controlled temperature program in a controlled environment, the weight change of a material is measured as a function of time or temperature [17]. It is supported that nanofillers could improve the thermal stability of the samples. An insulator and mass transport barrier to the small molecules produced during decomposition and thermal decomposition of the polymer matrix of blends measured by using TGA analysis. TGA was used to study the

impact of nanofillers on the thermal behaviours of the nanocomposites and blend, and it was found through TGA thermograms can help to better understanding of thermal stability of material.

### 2.3.6 Fourier Transform Infrared (FT-IR) Spectroscopy

Using Fourier Transform Infrared Spectroscopy - Attenuated Total Reflectance (FTIR-ATR), the chemical structure of polymer materials may identify, as well as the presence or absence of particular functional groups. Changes in the relative band strength and frequency of the absorption bands point to changes in the sample's chemical composition or surroundings. Therefore, FTIR-ATR spectroscopy may used to analyze the surface chemistry that results, particularly after chemical or physical modifications have been generated. The processing of FTIR spectroscopic data was done using a Bruker ALPHA II small FTIR spectrometer connected to a computer at GIRDA, Vadodara, India. ATR disc technique FTIR spectra of pure and blend of polymer at varied concentrations were conducted at ambient temperature with a wavenumber range of  $400\text{ cm}^{-1}$ -  $4000\text{ cm}^{-1}$  [18].

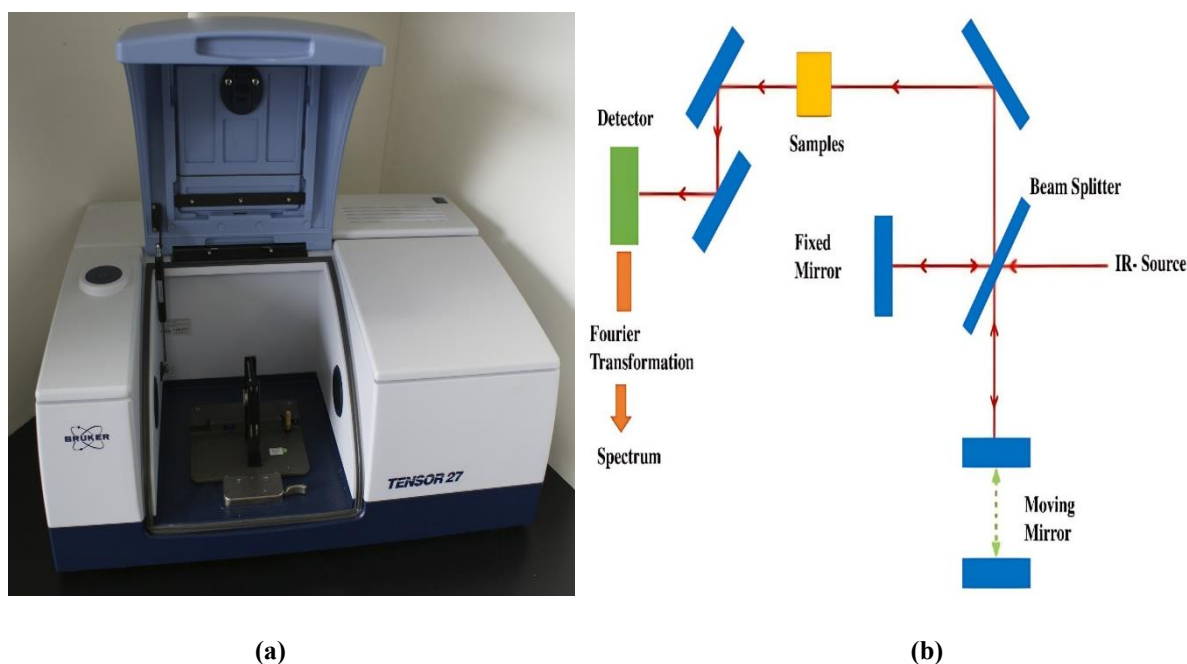


**Figure 2.8:** (a) FTIR-ATR instrument and (b) Schematic of FTIR-ATR instrument

The working principle of FTIR-ATR spectrometer is based on Michelson interferometer and schematically represented in Figure 2.8 (b). A poly-chromatic beam of IR radiations from the source is directed to a beam splitter after passing through a collimator. Each half of this beam is then focused on a moving and fixed mirror respectively. Due to the

movement of the mirror, incident half beam is blocked periodically and when it is recombined with the other half of the beam, it causes interference. This can be either constructive or destructive due to continuous change in the path length depending on the speed of the moving mirror. The intensities of all of the interferences created by each wavelength in the incident beam is summed up and then plotted against optical path difference. This intensity versus optical path difference plot is called ‘interferogram’. A fourier transformation is then applied to this interferogram to obtain resultant infrared spectra in intensity versus wavenumber form. Different techniques can be used to perform FTIR analysis [19].

### 2.3.7 Mechanical Properties

Figure 2.9 shows the shape of the tensile specimen used in this study and the static tensile test setup. The specimen had a length of 400 mm, width of 100 mm, and thickness of 25 mm. It had a dumbbell shape with a cross-section of 25 mm × 50 mm at its center. Both ends of the specimen were reinforced with two wire meshes to prevent the specimen from fracturing outside the strain measurement range (i.e., gauge length). To eliminate the effect of the specimen size, specimens of the same size were used in both the static tensile test and high-speed tensile test. Five specimens were evaluated at each specimen level [20].

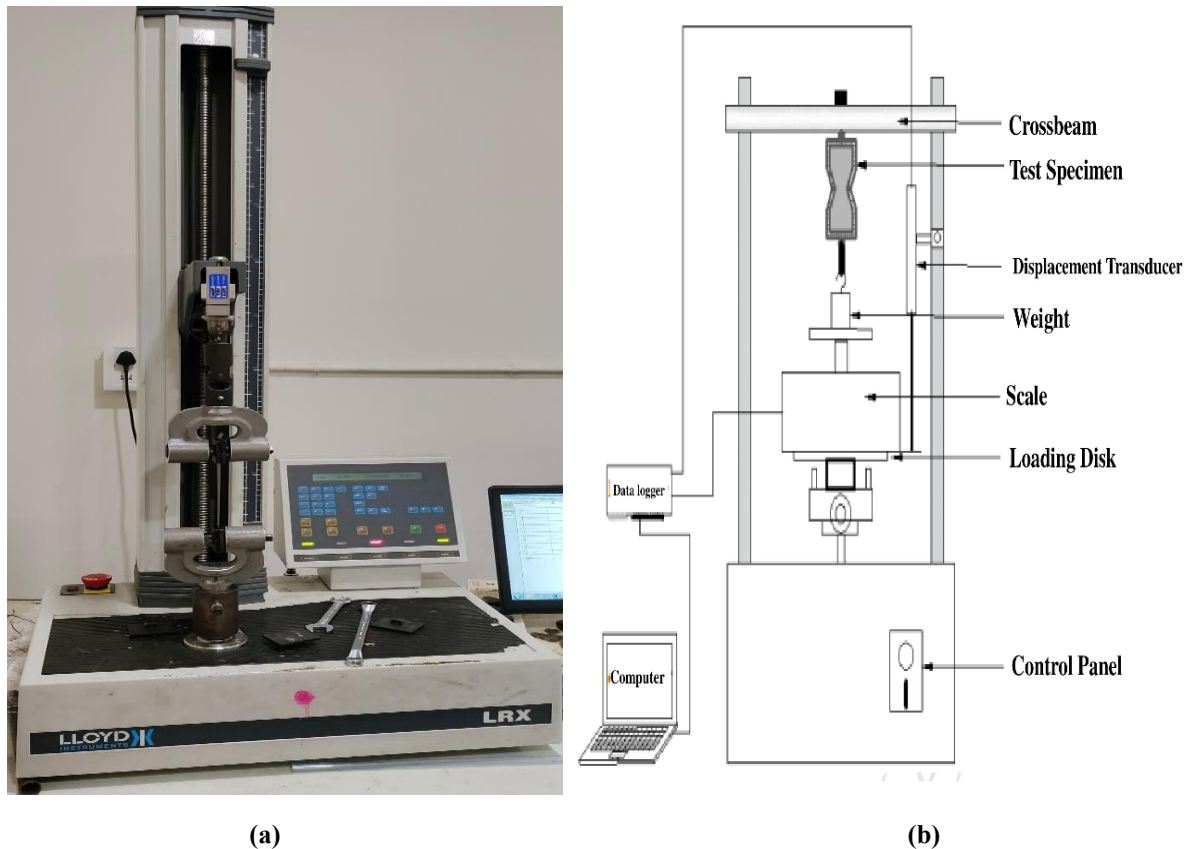


Figure 2.9: (a) Tensile strength instrument and (b) Schematic of tensile strength instrument

In order to measure the tensile strength, Young's modulus, elongation at break, and flexural strength of a material, tensile and flexural tests were performed on a Llyord EZ 20kN tensile tester at crosshead speeds of 10 mm/min and 3 mm/min, in our Faculty, respectively. A Zwick/Roell HIT-25P Izod impact tester was put through an Izod impact test utilizing an 11 J hammer, in our faculty. A Zwick/Roell automated notching machine was used to grind the samples notches at a 45° angle, 2.5 mm depth, and 0.25 mm radius. Each sample was tested (3 times), and average results were given under tensile stress until failure and a stress-strain curve were obtained. The polymeric material is a linear elastic solid at relatively low stresses and strains. The proportionate limit is the point at which the behaviour becomes non-linear. The yield point is the local maximum in the stress-strain curve that shows persistent deformation. Yield strength and elongation at yield are equivalent to stress and elongation. The material expands out significantly beyond the yield point, and this area is referred to as the plastic region. Further elongation results in strain hardening and ultimately causes the material to break. A number of factors, including temperature, strain rate, microstructure, and molecular properties, influence a polymeric material's stress-strain behaviour [21].

### 2.3.8 X-ray Diffraction (XRD)

X-ray diffraction (XRD) analysis has the advantage that materials can be reused, and it can be performed quickly. X-rays are electromagnetic waves that appear by converting the kinetic energy of the original electrons when fast-moving electrons are rapidly decelerated or stopped under the influence of metal atoms. When these X-rays are incident on a certain material, the scattered waves from each atom interfere with each other, and diffracted waves are generated only in a specific direction. X-ray analysis uses the diffraction of X-rays to confirm structural information, such as the chemical composition, crystal structure, and crystal size of materials. X-ray equipment consists of an X-ray tube (X-ray generator), goniometer, monochromator, detector, control/data processing unit, etc.

X-rays are incident on the sample, the incident angle is changed using a goniometer, and the scattered X-rays are monochromatized through a monochromator and detected using a detector. Through the detected X-ray information, various structural information about the material, such as the crystallinity, chemical composition, crystal structure, and crystalline size, can be obtained [22]. The X-ray analysis of pure and blends polymer thin films was also obtained.



**Figure 2.10:** X-ray diffraction instrument (smartLab SE)

The X-ray (Rigaku Smartlab SE) instrument, in our department, MSU, baroda, which is shown in Figure 2.10. The X-ray instrument with Ni-filtered  $\text{Cu}_{K\alpha}$  radiation of wavelength  $1.5406 \text{ \AA}$  was used to record X-ray diffraction spectra of pure polymers, blend of polymers, and blend composites polymer structural analysis. The X-ray images were captured at  $5^\circ/\text{min}$  in  $0.02^\circ$  increments, covering a two range of  $4^\circ$ - $80^\circ$ . The operational parameters were 30 kV and 15 mA was used for structural analysis by using the software smart Studio II. The most of the peak sites corresponded with the standard membranes structure data. The crystalline size was calculated using the Debye-Scherrer formula, which is expressed through equation (2.7) [23]:

$$\theta = \frac{0.9 \lambda}{\beta \cos \theta} \quad (2.7)$$

Where  $\theta$  = diffraction angle in radian,  $\lambda$  = X-ray wavelength ( $1.5406 \text{ \AA}$ ) and  $\Theta$  = particle diameter.

### 2.3.9 Field Emission Scanning Electron Microscopy (FE-SEM)

FE-SEM is one of the high-resolution electron microscopy techniques, FE-SEM uses an electron beam to probe a sample at an extremely fine scale to reveal additional in depth about nanomaterials. The size, size distribution, generation, and shape of produced micro- and nano-zines may all be closely monitored using this surface imaging technique. This current method used measures from the histogram, obtained either manually or via various types of specified software, to analyze the morphology of the polymer membrane samples, an FE-SEM model known as the Nova Nano FE-SEM 450 (FEI), MNIT, Rajsthan, India, was used, which is shows in Figure 2.11 (b).

The samples were frozen using liquid nitrogen and then broken into small pieces to suit the specimen chamber. Then, the holders were attached to the smaller parts [24]. Electrons are produced at the top of the column in the electron gun and accelerated through the column at a specified accelerating voltage (1 keV – 30 keV).

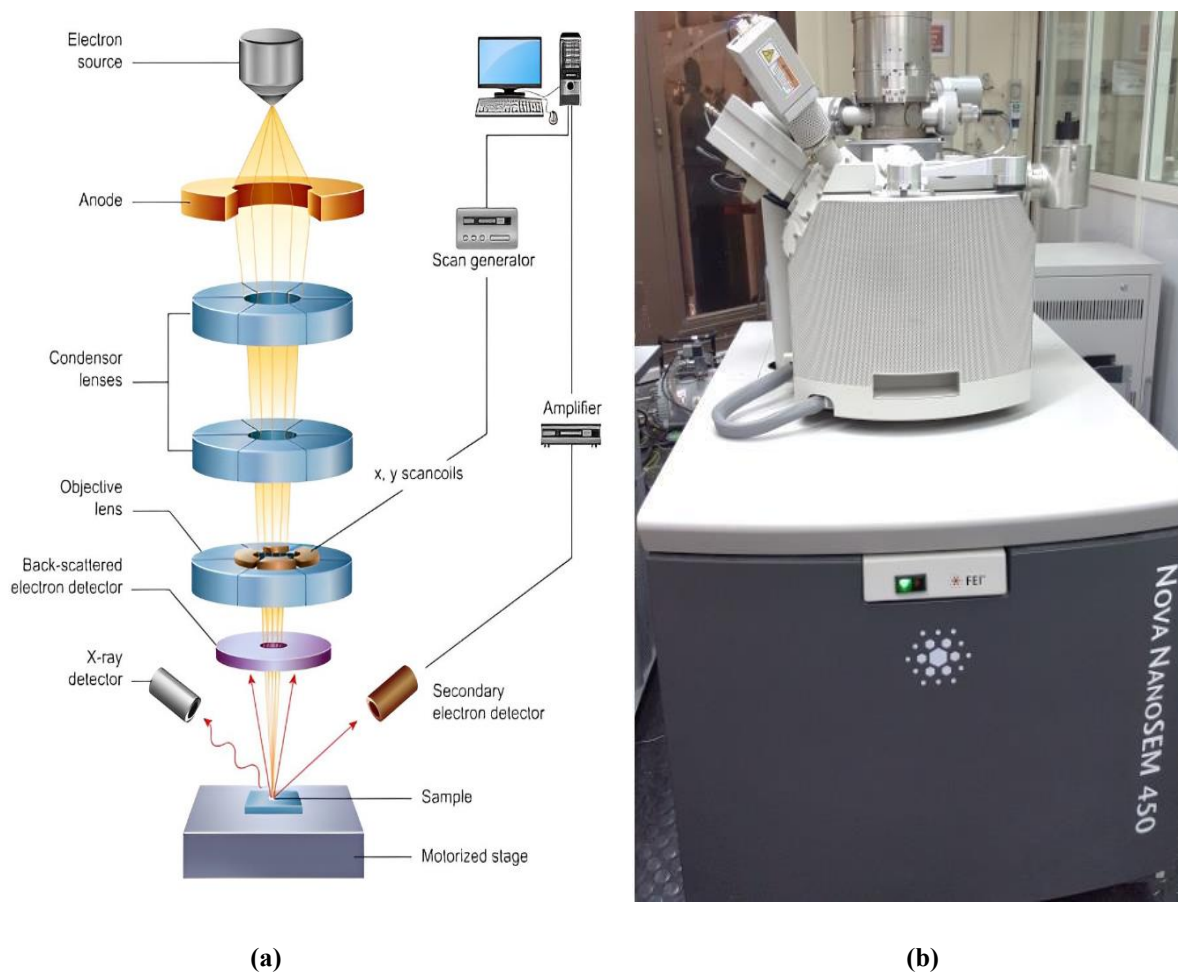


Figure 2.11: (a) Schematic of FE-SEM instrument and (b) FE-SEM instrument

Condenser lenses and apertures act to reduce the beam diameter. The final lens in the column is the objective lens, which focuses the beam on the sample surface. The diameter of the beam in an SEM can range from <1 nanometer up to 20 nanometers, depending on the type of electron gun, accelerating voltage, and lens configuration. The sample itself is mounted on a stage in the chamber area and both the column and the chamber are maintained under vacuum by a combination of pumps.

The level of the vacuum will depend on the design of the microscope. Some microscopes allow for variable pumping, allowing the sample chamber to be kept at a lower vacuum level than the rest of the column in order to support low-vacuum imaging the position of the electron beam on the sample is controlled by scan coils situated above the objective lens. These coils allow the beam to be scanned over the surface of the sample in the X-Y plane. The scanned beam strikes the sample, generating a variety of signals including secondary electrons, backscattered electrons, and characteristic X-rays. These signals are then detected by appropriate detectors [25].

### 2.3.10 UV-Visible Spectroscopy

A UV-Visible (UV-Vis) spectrophotometer is an analytical instrument used to measure the absorption or transmission of ultraviolet (UV) and visible light by a sample. Principle of operation, the basic principle involves the absorption of light by a sample. When a beam of UV or visible light passes through a sample, some of the light is absorbed by the sample's molecules. The amount of absorption is indicative of the sample's concentration.

This experiment used Thermo Scientific UV-Spectroscopy Model Evolution 600 UV-Vis, in our department and data analysis by VisionPro software. The scanning wavelength range is 200 nm - 900 nm. The thicknesses of membranes range from 60  $\mu\text{m}$  to 70  $\mu\text{m}$  [26].

### 2.3.11 Contact Angle Analysis

The membrane surface's hydrophilic and hydrophobic behaviour is determined using the contact angle (CA) measurement shows in Figure 2.12 (a). Contact angle measurement is used to examine the impact of surface treatment on the membrane during research and development processes such as coating, chemical cross-linking, and functionalization. It is possible to analyze the contact angle of the sample surface using a variety of media, including alcohol, water, and other solvents.

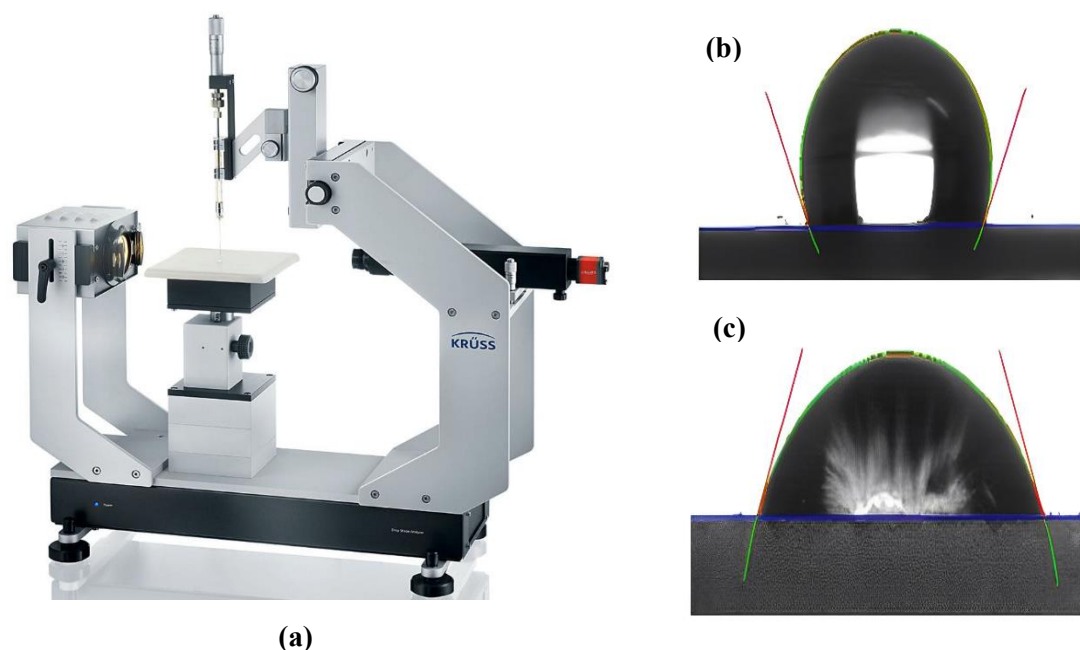


**Figure 2.12:** (a) Contact angle measurement instrument, (b) Contact angle images of hydrophobic (c) Hydrophilic surface of the membranes

Contact angle analysis is a technique used to measure the contact angle formed between a liquid droplet and a solid surface. Contact angle measuring instrument, DSA30 series, Smartech Inc., Vadodara, India. This analysis provides valuable information about the wetting behaviour of a liquid on a solid substrate, offering insights into surface properties such as surface energy, roughness, and cleanliness.

The measurement is particularly useful in fields such as material science, surface chemistry, and biology. The contact angle is the angle formed between the tangent to the liquid droplet at the point of contact and the solid surface. In material science the optimizing surface properties for adhesion or repulsion. Ensure the solid surface is clean and dry, the droplet placement, place a small droplet of the liquid of interest onto the solid surface. Image capture, capture an image of the droplet on the surface. Analysis, use specialized software to analyze the droplet shape and determine the contact angle [27].

Above characterization techniques have been used in next chapters to investigate the properties of various membrane. The membrane materials used for present thesis work are classified in a different chapters.

## References:

- [1] Z. Dai, L. Ansaloni, L. Deng, Recent advances in multi-layer composite polymeric membranes for CO<sub>2</sub> separation, *A review, Green Energy Environ*, **2016**, 32, 102–128.
- [2] B. A. Mccool, Y. S. Lin, Nanostructured thin palladium-silver membranes: Effects of grain size on gas permeation properties, *J. Mater. Sci.*, **2001**, 12, 3221–3227.
- [3] N. K. Acharya, Temperature-dependent gas transport and its correlation with kinetic diameter in polymer nanocomposite membrane, *Bull. Mater. Sci.*, **2017**, 40, 537–543.
- [4] A. K. Patel, N. K. Acharya, Metal coated and nanofiller doped polycarbonate membrane for hydrogen transport, *Int. J. Hydrogen Energy*, **2018**, 43, 21675–21682.
- [5] Y. K. Vijay, S. Wate, N. K. Acharya, J. C. Garg, The titanium-coated polymeric membranes for hydrogen recovery, *Int. J. Hydrogen Energy*, **2002**, 27, 905–908.
- [6] M. Salimi, V. Pirouzfard, E. Kianfar, Novel nanocomposite membranes prepared with PVC/ABS and silica nanoparticles for C<sub>2</sub>H<sub>6</sub>/CH<sub>4</sub> separation, *Polym. Sci. - Series A*, **2017**, 59, 566–574.
- [7] J. Ahn, W. J. Chung, I. Pinnau, M. D. Guiver, Polysulfone/silica nanoparticle mixed-matrix membranes for gas separation, *J. Memb. Sci.*, **2008**, 314, 123–133.
- [8] M. J. Han, S. T. Nam. Thermodynamic and rheological variation in polysulfone solution by PVP and its effect in the preparation of phase inversion membrane, *J. Memb. Sci.*, **2002**, 202, 55–61.
- [9] S. M. Momeni, M. Pakizeh, Preparation, characterization and gas permeation study of PSF/Mgo nanocomposite membrane, *Brazilian J. Chem. Eng.*, **2013**, 30, 589–597.
- [10] A. C. Sun, W. Kosar, Y. Zhang, X. Feng, Vacuum membrane distillation for desalination of water using hollow fibre membranes, *J. Memb. Sci.*, **2014**, 455, 131–142.
- [11] A. M. Kansara, V. K. Aswal, P.S. Singh, Preparation and characterization of new poly(dimethylsiloxane) membrane series via a ‘cross-linking’ reaction using monomolecular trichloro (alkyl) silane of different alkyl chain and type, *RSC Adv*, **2015**, 5, 51608–51620.

- [12] X. Ding, Y. Cao, H. Zhao, L. Wang, Q. Yuan. Fabrication of high performance Matrimid/polysulfone dual-layer hollow fibre membrane for O<sub>2</sub>/N<sub>2</sub> separation, *J. Memb. Sci.*, **2008**, 323, 352-361.
- [13] J. A. Otero, O. Mazarrasa, J. Villasante, V. Silva, P. Pra danos, J. I. Calvo, A. Hernandez, Three independent ways to obtain information on pore size distributions of nanofiltration membranes, *J. of Memb. Sci.*, **2008**, 309, 17–27.
- [14] A. M. Efimov, V. G. Pogareva and A. V. Shashkin, Water-related bands in the IR absorption spectra of silicate glasses, *J. Non-Cryst. Solids*, **2003**, 332, 93.
- [15] K. Boussu, B. Van der Bruggen, A. Volodin, J. Snauwaert, C. Van Haesendonck, C. Vandecasteele, Roughness and hydrophobicity studies of nanofiltration membranes using different modes of AFM, *J. of Colloid Interface Sci.*, **2005**, 286, 632–638.
- [16] Q. Li, X. Pan, C. Hou, Y. Jin, H. Dai, H. Wang, X. Zhao, X. Liu, Exploring the dependence of bulk properties on surface chemistries and microstructures of commercially composite RO membranes by novel characterization approaches, *Desalination*, **2012**, 292, 9-18.
- [17] S. Pisana, M. Lazzeri, P. Casiraghi, Breakdown of the adiabatic Born-Oppenheimer approximation in graphene, *Nature Material*, **2007**, 6, 198-201.
- [18] M. Lucchese, F. Stavale, E. Ferreira, Quantifying ion-induced defects and Raman relaxation length in graphene, *Carbon*, **2010**, 48, 1592-1597.
- [19] G. Camino, S. M. Lomakin, M. Lazzari, Polydimethylsiloxane thermal degradation Part 1. Kinetic aspects, *Polymer*, **2001**, 42, 2395–2402.
- [20] S. K. Shukla, R. K. Tiwari, A. Ranjan, A.K. Saxena, G.N. Mathur, Some thermal studies of polysilanes and polycarbosilanes, *Thermochimica Acta.*, **2004**, 424, 209–217.
- [21] A. N. Chaudhry, N. C. Billingham, Characterisation and oxidative degradation of a room-temperature vulcanised poly(dimethylsiloxane) rubber, *Polymer Degradation and Stability*, **2001**, 73, 505–510.
- [22] M. I. Aranguren, Crystallization of polydimethylsiloxane: effect of silica filler and curing, *Polymer*, **1998**, 39, 4897-4903.

- [23] J. Lue, S. W. Yang, Sorption of Organic Solvents in Poly(DimethylSiloxane) Membrane. I. Permeant States Quantification using Differential Scanning Calorimetry, *Journal of Macromolecular Science, Part B: Physics*, **2005**, 44 711–725.
- [24] J. Lue, S. W. Yang, S. Chang, Sorption of Organic Solvents in Poly(Dimethyl Siloxane) Membrane. II. Effect of Sorption on the Polymer Crystals upon Cooling, *Journal of Macromolecular Science, Part B: Physics*, **2006**, 45, 417–430.
- [25] N. Widjojo, T. S. Chung, Thickness and air gap dependence of macrovoid evolution in phase-inversion asymmetric hollow fibre membranes, *Ind. Eng. Chem. Res.*, **2006**, 45, 7618-7626.
- [26] R. S. Murali, T. Sankarshana, S. Sridhar. Air separation by polymer based membrane technology, *Separation & Purification Reviews*, **2013**, 42, 130-186.
- [27] G. Dong, H. Li, V. Chen. Challenges and opportunities for mixed-matrix membranes for gas separation. *J. of Materi.Chem. A*, **2013**, 1, 4610-4630.